Petrofabric Analysis of a Drag Fold

By

Ikuo HARA

with 31 Text-figures and 2 Plates

ABSTRACT: A simple type of a drag fold of siliceous phyllite found in the Sangun metamorphic formation near the Nakase mine, Hyogo Pref., Western Japan, has been analysed with reference to the mica fabric, the quartz c-axis fabric and the quartz lamellae fabric, and the stress and movement picture in the deformation related to the latter two have been discussed. The stress and movement picture through the fold (drawn with reference to those fabric elements) have been fairly well correlated with those in the experimental bending of sheets. The petrofabric technique of fold analysis after J. LADURNER (1954a) seems not always to be available for synthesis of the mechanics of folding even when a single marked maximum occurs in the c-axis diagram prepared in each sector of the fold. The rule of the establishment of the stess system (the axis of maximum compressive stress and that of maximum tensile stress) with respect to the lamellae inclined at moderate to low angles to the c-axis of quartz has been also discussed.

CONTENTS

I. INTRODUCTION

From informations concerning the mechanics of folding of a sheet based on theoretical and experimental investigations, the stress and strain picture in rock folding, even if the rock involved in the fold in question is of homogeneous non-stratified rock, are heterogeneously distributed through the folded rock. The rock fold is generally of the multiple-layered system made of the superposition of layers having different thickness and physical properties. Owing to such nature of the lithic unit involved in the fold, the stress system acting on it during folding under a given external force must be further remarkably complicated, that resulting in heterogeneous development of fabric elements of various types through the fold. Since B. SANDER (1930) had reported his classic petrofabric studies about small-scale folds of the rocks of various types in Tyrol, petrofabric analyses of folds have been made by many workers (E. INGERSON, 1940; SANDER, 1950; LADURNER, 1954 a and b; I. S. ZOZMANN, 1955; K. A. JONES, 1959; T. K. BALL, 1960; etc.). And nowadays, generally, the petrofabric analyses of rock folds have been done with

reference to LADURNER's method well known. However, discussions on the mechanics of folding seem to have been commonly based on the petrofabric analysis about some particular layers in the multiple-layered lithic unit involved in the fold. This seems to be disadvantageous to synthesize the stress and strain picture in folding of the multiple-layered system.

In the Sangun metamorphic formation near the Nakase mine, Hyogo Pref., Western Japan, has been found a drag fold of siliceous phyllite, a multiple-layered system made of the superosition of quartz-rich layers and mica-rich layers, in which the quartz lamellae were well developed. In this paper the stress and movement picture in the deformation related to the lamellae through the drag fold have been examined according to the author's rule of the establishment of the stress system in the deformation which produced the quartz lamellae (HARA, 1961a). The author (1961a) pointed out that the c-axis of quartz may stably be oriented at an angle of ca. 30° to the greatest contraction axis in the system concerned, or of ca. 60° to the greatest extension axis. On the basis of this hypothesis, the strain picture for the c-axis fabric through the fold has also been discussed.

Acknowledgements: The author takes great pleasure in submitting this article for publication in the memorial volume dedicated to Prof. YOSHIO KINOSAKI. The author wishes to record his sincers thanks to Prof. G. KOJIMA for his kind advices and reading the manuscript. Acknowlegements are due to Dr. K. HIDE for his kind suggestions to the study. Thanks are also due to the members of the Petrologist Club of the Hiroshima University for their valuable discussions. Finally the author acknowleges with gratitude that a part of expense for this research was defrayed by the Grant in Aid for Scientific Researches from the Ministry of Education, Japan.

II. STYLE OF FOLD

The rock involved in the fold examined in this paper is phyllite derived from siliceous shale. It consists mainly of quartz, muscovite, and graphitic matter, accompanied with subordinate chlorite and albite, and is characterized by a single distinct foliation defined by alternation of mica-rich layer and quartz-rich layer, that defines the form of the fold, and by a distinct lineation parallel to the axis of the fold.

Fig. 1 is a schematic sketch of profile of the fold. It shows a zone in which layers are folded in acute form (folded zone) and two zones in which layers are not folded in acute form but gently waving (non-folded zone). The former zone is intercalated in the latter. The fold in question corresponds to it in the former zone. The boundary lines between the folded zone and non-folded zones are clearly drawn along two thick mica-rich layers, as shown in Fig. 1. This fact suggests that those two mica-rich layers acted as a surface of décollement which means the detachment of the folded zone from the surrounding non-folded zones.

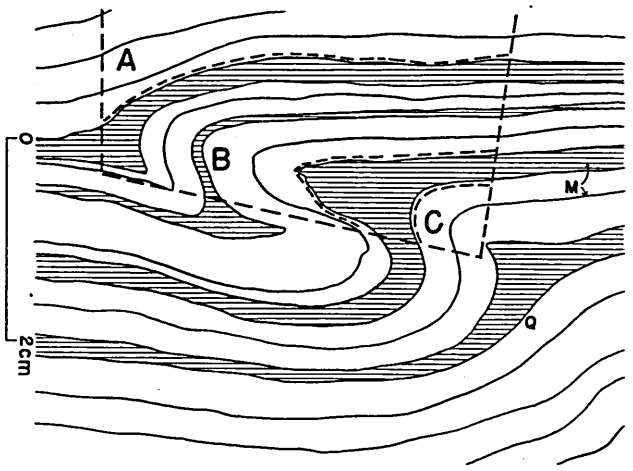

FIG. 1 Schematic skecth of the specimen.
M : mica-rich layer. Q : quartz-rich layer. A, B and C : three subareas.

From the presence of the surfaces of décollement, it may be pointed out that layers the of folded zone bounded by them must have moved and took their structure independently of the surrounding non-folded layers (*cf.* De SITTER, 1956).

Briefly speaking, the structure in the folded zone is defined in terms of two knees and three limbs, which consist of two limbs lying down parallel to the surrounding non-folded layers and one short limb connecting two knees (Fig. 1). The style of fold in question is of a drag fold, having macroscopically monoclinic symmetry with a single symmetry plane normal to the fold axis. Detailed petrofabric analyses were done about upper half part of the profile shown in Fig. 1.

Mica flakes occurring sporadically in the quartz-rich layers are oriented more or less parallel to the form surface of the fold, and no transversal structural surface is present (Plate 55–2). [001]-Axis fabric for mica flakes in the quartz-rich layers was examined, and with reference to the mica fabric the examined area was divided into three homogeneous subareas, that is, subarea A, B and C in Fig. 1. Subarea A corresponds to the non-folded zone, and subarea B and C to the folded zone. Mica fabrics in those subareas are illustrated in Figs. 2, 3 and 4. They together are characterized by a sharply defined great circle girdle, showing monoclinic symmetry with a single symmetry axis normal to the girdle. The single symmetry axis in each diagram represents the fabric axis *b* with reference to the mica fabric in each subarea, and in subarea B and C it must be correlated with the axis of the fold in question. The fabric axis *b* for the mica fabric in subarea A is found to be parallel to that in subarea C. However, the fabric axis *b* in these subareas does not coincide with that in subarea B, showing angular deviation of ca. 20°. Therefore, strictly speaking, the fold in question has a triclinic symmetry as a whole, unlike macroscopic monoclinic appearance. The boundary between subarea B and C is clearly drawn along a thick mica-rich layer (layer d in Plate 54–1), like that

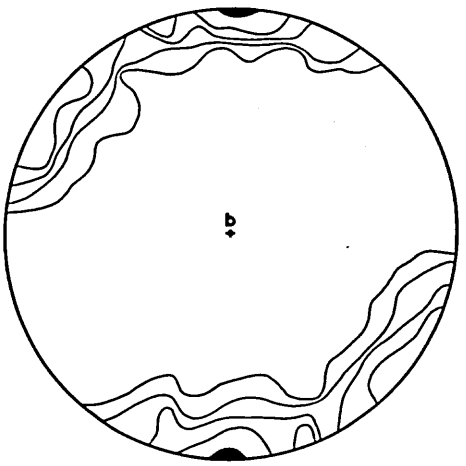

FIG. 2 [001]-axes of 200 mica flakes in subarea A.

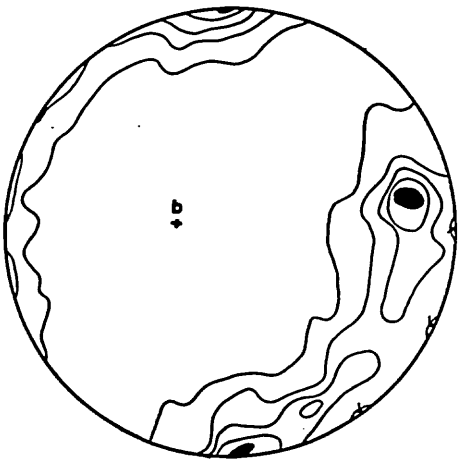

FIG. 3 [001]-axes of 100 mica flakes in subarea B.

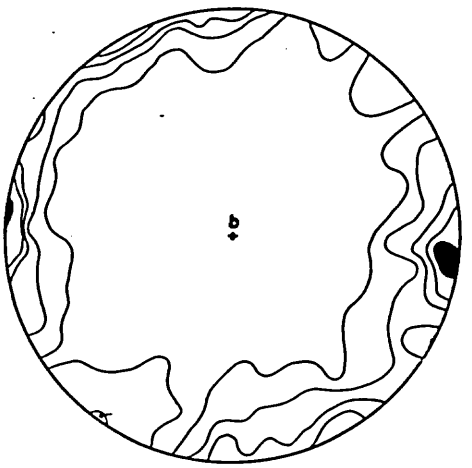

FIG. 4 [001]-axes of 100 mica flakes in subarea C.

between subarea A and B. Therefore, the fold with a triclinic symmetry in question can be divided into two units of fold with monoclinic symmetry, that is, the fold I corresponding to subarea B and the fold II to subarea C. The fabric axis *b* for the mica fabric in subarea B must be strictly identical with the axis of the fold I and that in subarea C with the axis of the fold II. In the innermost knee of the fold I the direction of curvature of the layer e is reversed with reference to the general direction of curvature of the fold I (Plate 55–1 and 2).

Generally speaking, triclinic fabrics result from either a single inhomogeneous strain or superposed genetically unrelated strains with higher symmetry. From the features of the fold in question above mentioned, the triclinic nature of the fold seems to have been resulted from a single inhomogeneous strain, and the

mica-rich layer d acted as a horizon of detachment between the fold I and fold II.

The thickness of mica-rich layers involved in the fold[1], measured radially, is not always constant (Plate 54–1 and Plate 55–1). That of the mica-rich layers b, j, l, n and p, which are involved in the outer knees of the fold I and fold II, is rather constant. While the mica-rich layers d, f and h, which are involved in the inner knee of the fold I, are remarkably thickened towards the axial part of the knee. In these mica-rich layers d, f and h slip cleavages which traverse the foliation surface at various angles are observed (Plate 54–1 and Plate 55–1). The transversal slip cleavages develop through the fold in such fashion as shown in Plate 54–1. In the axial part of the inner knee, generally, they traverse at high angles the foliation surface, though in its innermost margin they tend to run rather subparallel to it (Plate 54–1). The cleavages on the limbs are subparallel to the foliation surface and continue to the outer margin of the knee, where they traverse it at moderate angles. The transversal cleavages in question do not cut across the adjacent quartz-rich layers. They are not observed in the mica-rich layers j, l, n and p, of the outer knee of the fold I, having rather constant thickness measured radially.

In some parts of the quartz-rich layers develop tiny cracks inclined at high angles to the foliation surface, cutting quartz grains sharply with no evidences of associating granulation or plastic deformation, (Plate 54–1). They are of the type of tension crack, and run approximately parallel to the axis of the fold I and that of the fold II. They are generally observed in limbs of the fold I and fold II, especially in parts close to their knees. Some cracks are filled with micaceous matter injected from the surrounding mica-rich layers (Plate 55–3).

III. Analysis of the Quartz Lamellae Fabric

Two types of lamellar structures have been recognized in quartz grains of the quartz-rich layers. Number of grains containing the lamellae is very small when compared with the total number of grains constituting the quartz-rich layers. However, no lamellae have been recognized in quartz grains occurring sporadically in the mica-rich layers.

One type of the lamellae is distinctly displayed as narrow bands of different lattice orientation across the host crystal, terminating within the grain boundaries (Plate 55–5). The lamellae of this type correspond to the Type L3, according to the author's classification of quartz lamellae (Hara, 1961b). The lamellae in question have an average width of 0.006 mm. Some boundaries between the lamellar and the host crystal are displayed as sharp but continuous change of extinction position, and others as discontinous change of it. The relative positions between the c-axis of the lamellar crystal and that of the host crystal

1) In the following pages, the term, "the fold", is used for the fold in question as a whole.

could be measured accurately in all of the grains containing the lamellae. The value of shift in the c-axis from the host crystal to the lamellar crystal ($C_H \wedge C_L$) in measured grains is between 2° and 16°, with a maximum between 3° and 8°, as shown in Figs. 5-a, 6-a and 7-a. The lamellae of this type are observed throughout subarea A, B and C.

Another type of the lamellae is defined by a closely spaced planar structure consisting of minute dark inclusions, that corresponds to the Type L1, that is, "BÖHM lamellae", (Plate 55–4). The lamellae of this type are observed only within a sharply restricted part of subarea A, where the lamellae of Type L3 are not observed.

The crystallographic location of the lamellae of Type L3 with respect to the lattice direction of quartz could not directly be measured, and only their trends on the thin section could be directly measured. From the X-ray studies of quartz grains exhibiting deformation features including undulatory extinction, deformation lamellae, marginal granulation and fracturing in naturally deformed rocks, BAILEY, *et al.* (1958) said, "... most of the quartz has deformed plastically by bend gliding. One of the three crystallographic a axis is always the major axis of bending, ...". If so, the rotational axis of shift in the c-axis from the host crystal to the lamellar crystal should coincide with the a-axis. In previous work about the lamellae of similar type the author (1961b) described an example for which the angular deviation of the pole of lamellae from the great circle, on which C_H and C_L lie together, is between 0° and 8°, with a strong maximum between 0° and 3°. In this case the angular deviation is not so large. Tentatively in this paper, therefore, the crystallographic location of the lamellae of Type L3 has been indirectly determined on the basis of assumption that the rotational axis of shift in

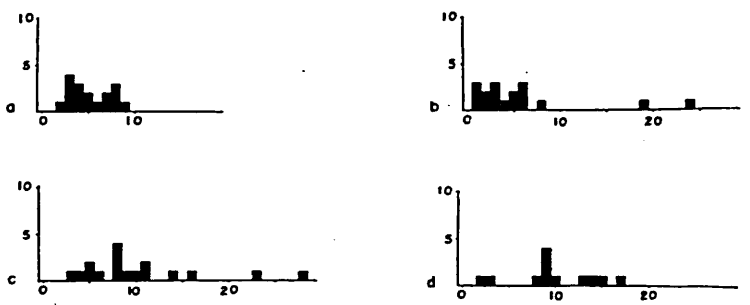

FIG. 5 a) Histogram showing the variation in the angle between the c-axis of host crystal and that of lamellar crystal. (for the lamellae of Type L3 in subarea A)
b) Histogram showing the variation in the angle between the c-axis of lamellar crystal and the pole of lamellae. (for the lamellae of Type L3 in subarea A)
c) Histogram showing the variation in the angle between the c-axis of host crystal and the pole of lamellae. (for the lamellae of Type L3 in subarea A)
d) Histogram showing the variation in the angle between the c-axis of host crystal and the pole of lamellae. (for the lamellae of Type L1 in subarea A)

the c-axis from the host crystal to the lamellar crystal coincides with the a-axis, according to the result of the X-ray studies of naturally deformed quartz grains after BAILEY, *et al.*

The crystallographic location of the lamellae of Type L3 was examined by measurment of angles between $L\perp$ and C_H and between $L\perp$ and C_L respectively (Figs. 5-b, 6-b, 7-b, 5-c, 6-c, and 7-c). The angle between $L\perp$ and C_H ($C_H \wedge L\perp$) is between 1° and 88°, that showing large variation of the crystallogrphic location of the lamellae. For many grains, however, $C_H \wedge L\perp$ is between 1° and 20°, that being similar to the results of SANDER (1930), FAIRBAIRN (1941), INGERSON and TUTTLE (1945), PRESTON (1958), CHRISTIE and RALEIGH (1959) and HARA (1961a and b). The angle between $L\perp$ and C_L ($C_L \wedge L\perp$) is between 0° and 83°, with a maximum between 1° and 20°.

Planes of the lamellae of Type L1 could be directly measured. The crystallographic location of the lamellae was examined by the measurment of angles between C_H and $L\perp$. $C_H \wedge L\perp$ is between 2° and 17°, that being similar to the case for the lamellae of Type L3 described above (Fig. 5-d).

The preferred orientation of the poles of lamellae for all grains containing the lamellae in subarea A is illustrated in Fig. 8-a. The poles of the lamellae of Type L1 and Type L3 are distributed together in the same part of the diagram. They are distributed in two sharply restricted areas, centers of which lie with angular

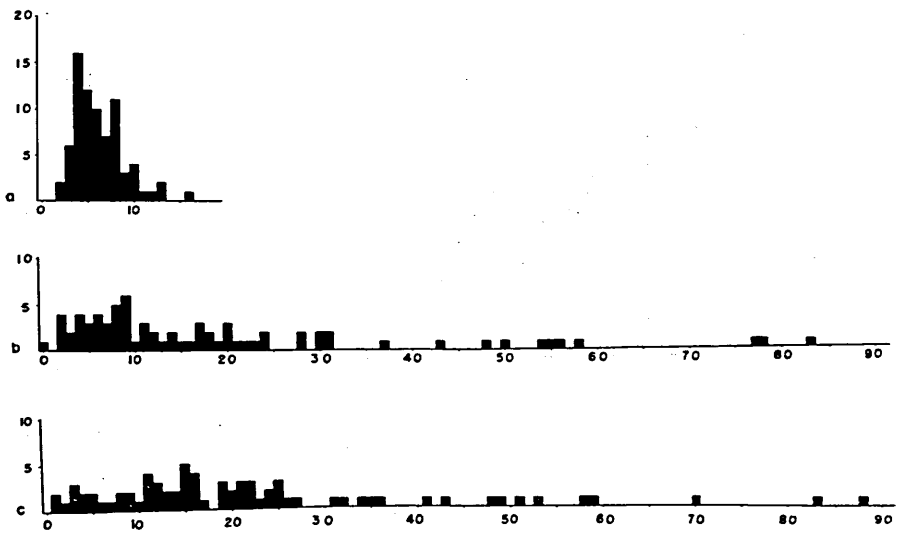

FIG. 6 a) Histogram showing the variation in the angle between the c-axis of host crystal and that of lamellar crystal. (for the lamellae of Type L3 in subarea B)
b) Histogram showing the variation in the angle between the c-axis of lamellar crystal and the pole of lamellae. (for the lamellae of Type L3 in subarea B)
c) Histogram showing the variation in the angle between the c-axis of host crystal and the pole of lamellae. (for the lamellae of Type L3 in subarea B)

distances of ca. 90° in the fabric plane *ac* for the mica fabric in this subarea, this fact indicating that the lamellae of these two types are tautozonally oriented and that they correspond approximately to two sets of (*h0l*)-planes with reference to the fabric axes for the mica fabric, which are roughly symmetrically oriented to the average trend of foliation surface (parallel to the fabric plane *ab* for the mica fabric) in subarea A. The L⊥ diagram shows almost perfect orthorhombic symmetry and the two symmetry planes coincide approximately with the fabric planes *ac* and *ab* for the mica fabric (Fig. 8-a). Therefore, the fabric axis *b* for the lamellae of those two types in subarea A coincides with that for the mica fabric.

The preferred orientation of the poles of the lamellae of Type L3 in subarea B is illustrated in Fig. 9-a. It is characterized by an incomplete great circle girdle normal to the fabric axis *b* for the mica fabric, and the lamellae in this subarea are also roughly tautozonally oriented. The L⊥ diagram shows a monoclinic symmetry with a single symmetry plane normal to the axis coinciding with the fabric axis *b* for mica fabric (the axis of the fold I), that is, the latter is identical with the fabric axis *b* for the lamellae fabric. Analogous pattern of the lamellae fabric is equally obvious for subarea C, as shown in Fig. 10-a. Also in subarea C the fabric axis *b* for the lamellae fabric coincides with that for the mica fabric (the axis of the fold II).

As mentioned in the preceding page, the rotational axis of shift in the c-axis from the host crystal to the lamellar crystal was assumed to coincide with the a-axis, according to the result of the X-ray studies of naturally deformed quartz grains after BAILEY, *et al.* Broadly speaking, in Figs. 8-b, 8-c, 9-b and 10-b the

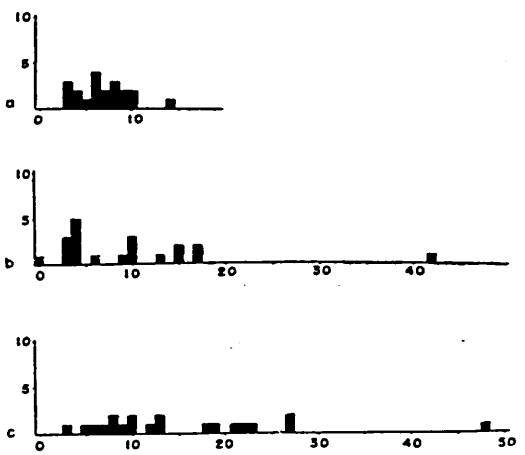

FIG. 7 a) Histogram showing the variation in the angle between the c-axis of host crystal and that of lamellar crystal. (for the lamellae of Type L3 in subarea C)
b) Histogram showing the variation in the angle between the c-axis of lamellar crystal and the pole of lamellae. (for the lamellae of Type L3 in subarea C)
c) Histogram showing the variation in the angle between the c-axis of host crystal and the pole of lamellae. (for the lamellae of Type L3 in subarea C)

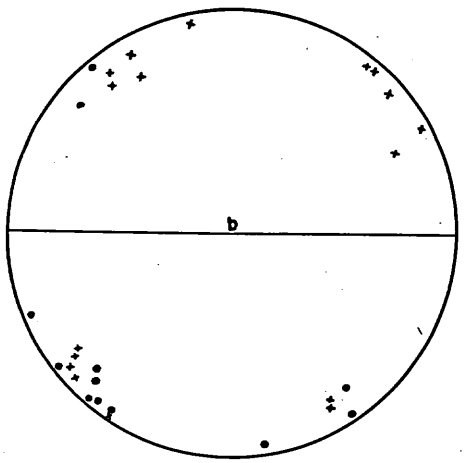

FIG. 8 a) Poles of lamellae in 29 grains (29 sets of lamellae) in subarea A. Dots represent the poles of the lamellae of Type L1 and crosses represent the poles of the lamellae of Type L3.

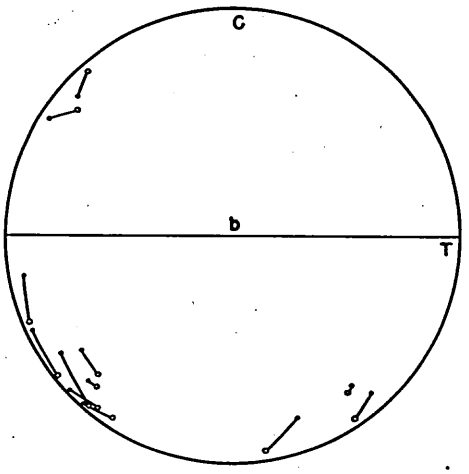

FIG. 8 b) Poles of the lamellae of Type L1 (circle) and c-axes of host crystal (dots) in 12 grains in subarea A.

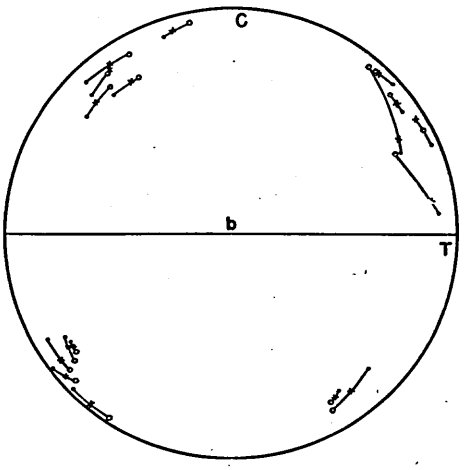

FIG. 8 c) Poles of the lamellae of Type L3 (circles) and c-axes of lamellar (crosses) and of host crystals (dots) in 17 grains in subarea A.

great circles containing C_H and C_L for grains with the lamellae of Type L3 and those containing C_H and $L\perp$ for grains with the Lamellae of Type L1 are parallel or subparallel to the *ac* great circle. This fact indicates that in each subarea the *b*-kinematic axis in the deformation related to the formation of the lamellae is parallel to the *b*-axis determined symmetrologically. In subarea A the *b*-kinematic axis for the lamellae of Type L1 seems to coincide with that for the lamellae of Type L3. Thus, discrepancy in the principal direction of movement between

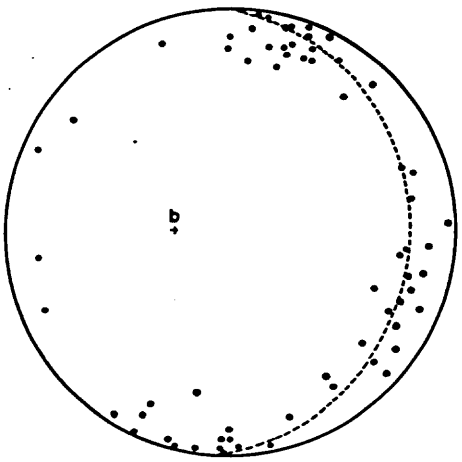

FIG. 9 a) Poles of the lamellae of type L3 in 64 grains (64 sets of lamellae) in subarea B.

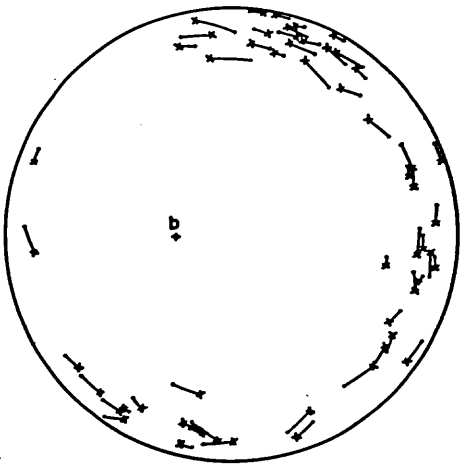

FIG. 9. b) c-Axes of lamellar crystals (crosses) and those of host crystals (dots) in 64 grains in subarea B.

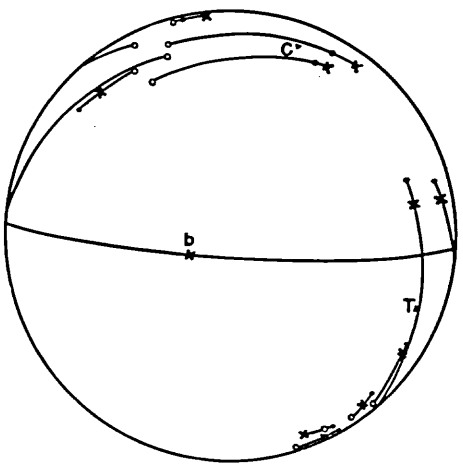

FIG. 9 c) Poles of the lamellae of Type L3 (circles) and c-axes of host (dots) and of lamellar cystals (crosses) in 10 grains in sector 5. C : axis of maximum compressive stress. T : axis of maximum tensile stress.

subarea B and subarea A and C drawn with reference to the mica fabrics can be done in quite similar fashion also with reference to the lamellae fabrics.

Plate 54–2 shows the distribution of quartz grains containing the lamellae through the fold and the trend of the lamellae in each grain, analysed on the thin section normal to the axis of the fold II. The development of the lamellae through the fold seems to be rather heterogeneous, that is, in the middle knees of the fold I and fold II the development are remarkable while in the outermost knees rather insignificant, as read in Plate 54–2. Although the variation in the trend of lamel-

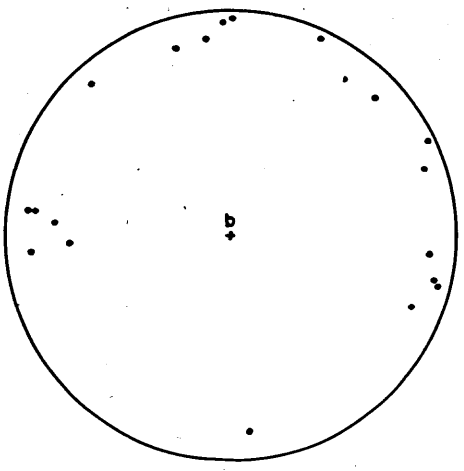

FIG. 10 a) Poles of the lamellae of Type L3 in 20 grains (20 sets of lamellae) in subarea C.

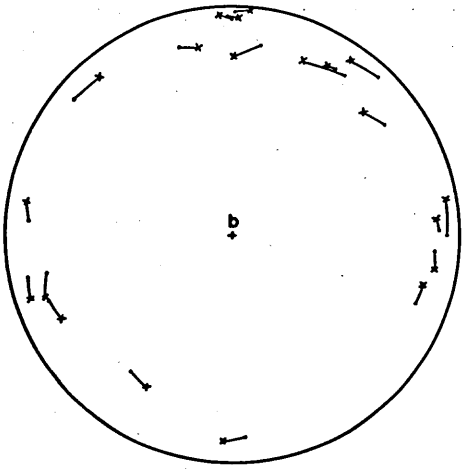

FIG. 10 b) c-Axes of lamellar crystals (crosses) and those of host crystals (dots) in 20 grains in subarea C.

lae is represented as an *ac* great circle girdle in the L⊥ diagrams, they do not seem to run at random through the fold, but to change regularly the trend in connection with the change of the position within the fold. The orientation pattern of the lamellae in subarea B and C is markedly different from that in subarea A, the latter being characterized by two maxima on the *ac* great circle in the L⊥ diagram.

According to the evidences described above, it is saflely concluded that also in the deformation related to the formation of the lamellae the mica-rich layers occurring between the fold I and non-folded zone (subarea A) and between the fold I and fold II acted as detachment horizons, that is, the layers involved in the fold moved independently of the surrounding non-folded layers, and further the layers involved in the fold I moved also independently of those involved in the fold II, as for the deformation related to the mica fabrics.

In detailed microscopic examinations of the experimentally deformed Yule marbles TURNER, *et al.* (1951) recognized a regular relationship between the development of $\{01\bar{1}2\}$ twin lamellae in calcite grains and the orientation of the lamellae with respect to the axis of applied force. TURNER (1953) pointed out successfully that this relationship may be available to locate the stress axes (compression and tension axis) related to the formation of the observed $\{01\bar{1}2\}$ twin lamellae in naturally deformed marbles. The present author (1961a) examined the lamellae in quartz with reference to the stress axes inferred with TURNER's method from the orientation of $\{01\bar{1}2\}$ lamellae in calcite in a naturally deformed calcite-quartz vein. Thereby, it was represented that the lamellae in quartz are grouped into two sets of planes, which are roughly symmetrically oriented with inclination of ca. 45° to the stress axes inferred from the $\{01\bar{1}2\}$ lamellae in calcite, and that

the lamellae in quartz are a kind of deformation band inclined at high angles to the active glide line. Furthermore the author pointed out that the relative positional relationships betwee C_H and C_L and between C_H and $L\perp$ in the composite diagrams for those axial data might be available to lacate the stress system in the deformation which produced the lamellae in quartz. The rule of the establishment of the stress axes (compression and tension axis) was said as follows:

"1) The pole of the lamellae in any grain is closer to the direction of the compressive stress than the c-axis of the host crystal in the same grain.

2) The c-axis of the lamellar crystal in any grain is closer to the direction of the compressive stress than the c-axis of the host crystal in the same grain.

3) Two groups of the poles of lamellae, distributed separately in angular distances of ca. 90° in the diagram for them, lie together on the plane containing the compression and tension axis.

4) The compression and tension axis are located to points which lie midway between two groups of the poles of lamellae on the great circle, on which these lie together."

According to the rule, in subarea A the stress axes in the deformation related to the formation of the lamellae of Type L1 is determined as shown in Fig. 8-b, that is, the point C corresponding to the compression axis and the point T to the tension axis. The axis of the compressive stress is approximately normal to the average trend of foliation surface (the fabric plane *ab*) and the axis of tensile stress is approximately parallel to that and normal to the fabric axis *b*. The same stress picture is drawn for the lamellae of Type L3, as shown in Fig. 8-c. It may be, therefore, pointed out that the lamellae of Type L1 and Type L3 were simultaneously formed under the same stress condition as described above. As mentioned in the preceding pages, in subarea A they do not coexist, unlike the example described by WEISS (1954). The lamellae of Type L1 develop only in a sharply restricted part of subarea A. For the lamellae of Type L3 with the same value of $C_H \wedge C_L$, some boundaries between the lamellar and host crystal are displayed as sharp but continuous change of extinction position, and others as discontinuous change of it. The author (1961b) pointed out that the lamellae of Type L1 were evolved from the lamellae of Type L3 under annealing condition with suitable chemical reagents, under which, on the boundary between the lamellar and host crystal, the polygonization wall was formed by the climbing of "dislocations" piled up in the glide planes, subsequently differential solution of silica along the polygonization wall took place, and fluid and solid inclusions were precipitated, that being quite similar to lines of etch-pits delineating polygonization walls perpendicular to the active glide planes observed in an aluminum crystal bent to 3 cm radius and annealed for 18 hr. at 625°C after R. W. Cahn (1949), (*cf.* J. E. Dorn, (editor), 1961). It may be, thus, pointed out that within subarea A the annealing condition in question was heterogeneous during and/or after the defromation related to the formation of the lamellae in quartz grains.

From above discussions, the assumption in this paper that the rotational axis of shift in the c-axis from the host crystal to the lamellar crystal for the lamellae of Type L3 coincides with the a-axis, according to the result of X-ray studies of naturally deformed quartz grains after BAILEY, *et al.*, seems to be justified. The rotational axis in question must be at least perpendicular or subperpendicular to the c-axis, like that for the lamellae of Type L3 previously examined by the author (1961b).

Fig. 9-c is the diagram for positional relationship between C_H, C_L and $L\perp$ for all grains containing the lamellae in sector 5 (Plate 54–5). The poles of the lamellae are distributed in a sharply restricted area, center of which lies on the *ac* great circle for the lamellae fabric in subarea B, this fact indicating that the lamellae correspond approximately to one set of the (*h0l*)-planes. In spite of such regular orientation of the lamellae through sector 5, the author's rule is not applicable to the positional relationships between C_H and C_L and between C_H and $L\perp$ in Fig. 9-c. The rule in question was established on the basis of careful examinations about the lamellae inclined at high angles to the c-axis. The lamellae in sector 5 are grouped into three types with reference to their crystallographic locations as follows: 1) the lamellae inclined at high angles to the c-axis, $C_H \wedge L\perp$ being between 2° and 19°, 2) the lamellae inclined at moderate angles to the c-axis, $C_H \wedge L\perp$ being between 47° and 51°, and 3) the lamellae inclined at low angles to the c-axis, $C_H \wedge L\perp$ being between 83° and 88°.

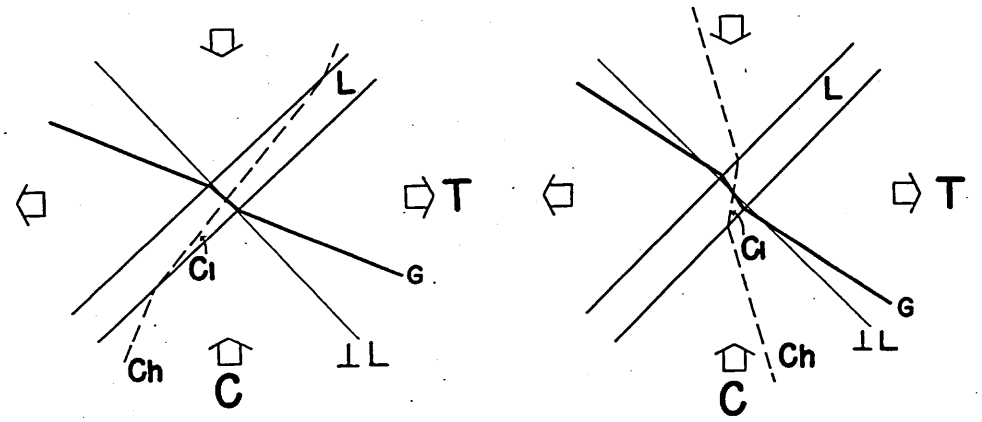

FIG. 11 Schematic sketch of relation of lamella (L), pole of lamella (⊥L), c-axis of lamellar crystal (Cl), c-axis of host crystal (Ch), assumed glide line (G), compression axis (C) and tension axis (T).

For the lamellae inclined at high angles to the c-axis in sector 5 the positional relationships between C_H and C_L and between C_H and $L\perp$ (with one exception) are regular in quite similar fashion to those for two specimens described previously by the author, as shown clearly in Fig. 9-c. With reference to those lamellae,

tentatively, the stress axes for the lamellae fabric in sector 5 was established. In Fig. 9-c the point C corresponds to the compression axis and the point T to the tension axis. For all the lamellae in sector 5, regardless their crystallographic locations, the rotational sense of shift in the c-axis from the host crystal to the lamellar crystal is the same, that is, clockwise on the plane of Fig. 9-c. Fig. 11 shows correlations between the shift in the c-axis from the host crystal to the lamellar crystal for the lamellae inclined at moderate to low angles to the c-axis and the stress axes established tentatively with reference to the lamellae inclined at high angles to the c-axis. Relationship among the lamella, C_H, C_L, and stress axes in Fig. 11 is quite similar to that for the lamellae inclined at high angles to the c-axis (see HARA, 1961a, Fig. 12). Therefore, the lamellae inclined at moderate to low angles to the c-axis may also be regarded as a kind of deformation band inclined at high angles to the active glide line, which lies possibly on any plane parallel to the crystallographic forms $\{10\bar{1}1\}$, $\{01\bar{1}1\}$ and $\{0001\}$ and be normal to the a-axis, like the lamellae inclined at high angles to the c-axis, which were regarded as a kind of deformation band inclined at high angles to the glide line parallel or subparallel to the c-axis. The possibility of translation gliding on the planes parallel to $\{10\bar{1}0\}$, $\{10\bar{1}1\}$, $\{01\bar{1}1\}$ and $\{0001\}$ has been discussed so far by many authors (MÜGGE, 1896; FISCHER, 1925; SCHMIDT, 1927; SANDER, 1930; HIETANEN, 1938; GRIGGS and BELL, 1938; FAIRBAIRN, 1949; WEISS, 1954; CHRISTIE and RALEIGH, 1959; etc.). Strictly speaking, however, any plane for translation and twin gliding in quartz was not determined apto now. However, the lamellae displayed as narrow bands of different lattice orientation across the host crystal (Type L3) can be reasonably regarded as a kind of deformation band inclined at high angles to a certain active glide line, on the basis of evidences which were described in this paper and the previous papers.

On the basis of above considerations, to the rule of the establishment of the stress axes in the deformation related to the formation of the lamellae in quartz must be added the following items:

1) The previous rule is applicable to the lamellae inclined at high angles to the c-axis. However, the establishment of the stress axes by refering only to the positional relationship between C_H and $L\perp$ in the diagram for these axial data seems to be in danger, because this relationship is not always regular in the diagram, as shown in Fig. 9-c.

2) Generally, the positional relationship between C_H and C_L in the diagram seems to be constantly available to establish the stress axes.

3) For the lamellae in any grain on which relative position between C_H and C_L can be measured, generally, the compression and tension axis are located on the great circle, on which $L\perp$, C_H and C_L lie (approximately) together, and at two points which are oriented with inclination of ca. 45° to the lamellae. Which points correspond to the compression axis or to the tension axis are determined with reference to the relationships in Fig. 11 and also in Fig. 12 of the previous

paper (1961a).

4) The lamellae having remarkably large value of $C_H \wedge C_L$ seem not to be available to the establishment of the stress axes.

As described in the preceding pages, the orientation pattern of the lamellae in the fold I and that in the fold II were represented as an *ac* great circle girdle in the $L\perp$ diagrams. Accordingly, the planes of the lamellae correspond approximately to the (*h0l*)-planes. The *b*-kinematic axis in the deformation related to the formation of the lamellae within the fold I and that within the fold II coincide respectively with the axis of the fold I and the axis of the fold II. The distribution of grains containing the lamellae through the fold I and fold II and the trend of the lamellae in each grain were analysed with the result of Plate 54–2 on the thin section normal to the axis of the fold II. The compression and tension axis responsible for the formation of the lamellae in each grain were established according to the author's rule and plotted on the section normal to the axis of the fold II (Plate 54–3), to which the plane containing those stress axes is approximately parallel. As is obvious in Plate 54–3, in the quartz-rich layers involved in the fold I and fold II the trends of the compression and tension axis in question are not constant, unlike those in subarea A described in the preceding page. In subarea A the stress axes were uniformly established in such fashion as the compression axis is approximately normal to the average trend of foliation surfaces and the tension axis is approximately parallel to it and normal to the fabric axis *b* (Fig. 8-b and c). In Plate 54–4 is shown schematically the distribution of the maximum compressive stress during the deformation related to the lamellae through the quartz-rich layers in subarea A, B and C on the basis of the data of Fig. 8-b and c and Plate 54–3. As mentiond in the preceding page, in quartz grains occurring sporadically in the mica-rich layers no lamellae have been recognized. Accordingly, the stress system acted through the mica-rich layers during the deformation related to the formation of the lamellae can not be drawn. In Plate 54–4, in the mica-rich layers are drawn dotted lines connecting lines of maximum compressive stress in neighbouring quartz-rich layers, by which the stress picture through the quartz-rich layers involved in the fold shall be more clearly visuallized, but the lines do not necessarily indicate real directions of maximum compressive stress through the mica-rich layers.

As mentioned in the preceding page, the fold in question is of a multiple-layered system made of the superposition of quartz-rich layers and mica-rich layers. Strictly speaking, all the layers are of different thickness and physical properties, either among quartz-rich layers or among mica-rich layers. The mica-rich layer and the quartz-rich layer have quite different rigidity, and, judging from various evidences described in the preceding pages, the former is remarkably softer than the latter. Those nature of the structural lithic unit involved in the fold suggests that the stress system acting on it during folding shall hot be simple. However, the lines of maximum compressive stress responsible for the lamellae through the

quartz-rich layers involved in the fold show a rather simple regular picture as shown in Plate 54–4.

With reference to Plate 54–4 it may be pointed out that the stress picture for the left side and that for the right side with reference to the axial plane of the fold are approximately symmetrical, that the stress picture for the fold I and that for the fold II are of quite identical fashion, and that the attitude of the lines of maximum compressive stress with reference to the form surface of the fold is distinctly different between the outer knee, the inner knee and the limb. Broadly speaking, in the outer knees and limbs of the fold I and fold II the lines of maximum compressive stress are approximately normal to the form surface, while in the inner knees they show moderate to low inclinations to it. In the axial part of inner knees they are parallel to the form surface. Passing from the outer knee to the inner knee, their trends show sharp but continuous change, and in the inner knees appear to be arcuated. In the limb close to subarea A the lines of maximum compressive stress are approximately trending parallel to those in this subarea, as shown in Plate 54–4.

Fig. 12 is the quartz lamellae fabric in a drag fold of a composite layer made

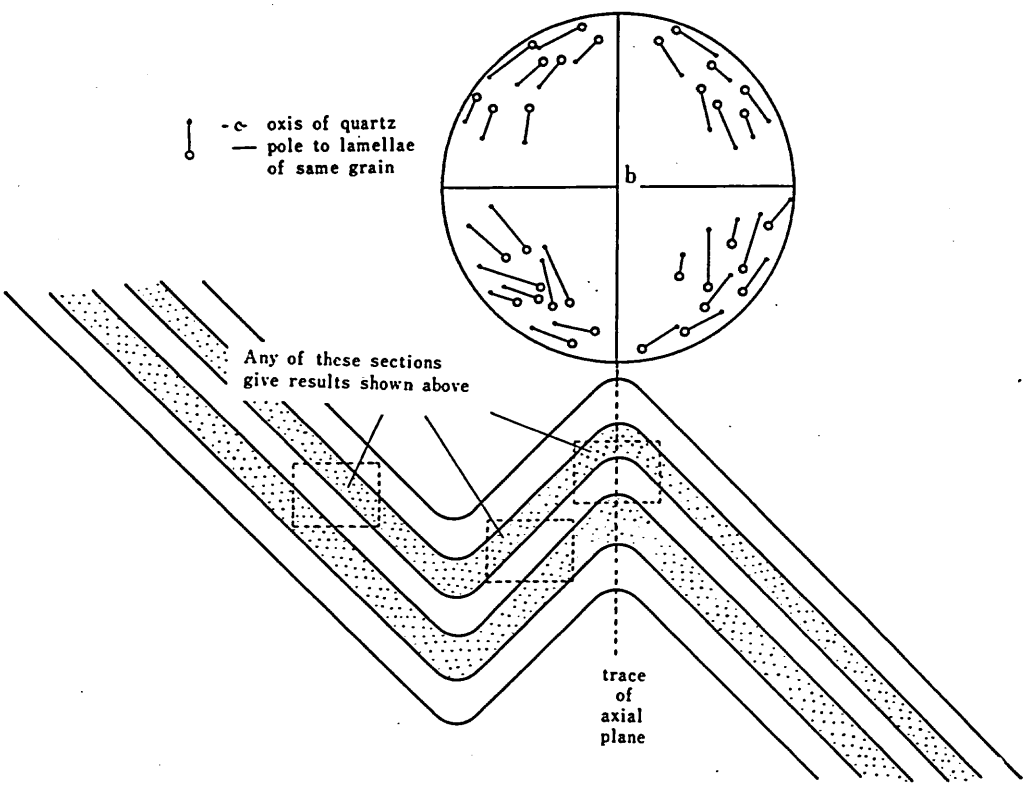

FIG. 12 Diagram illustrating the relation between the poles of lamellae (Type L1), c-axes of host crystals, and fold-axis of a small drag fold in mica schist. (after Tuttle, O. F., 1949).

of the superposition of quartz-rich layer and mica-rich layer described by O. F. TUTTLE (1949). The lamellae are of the Type L1. The center of the diagram coincides with the axis of the drag fold. The poles of lamellae are distributed in two sharply limited areas, centers of which lie with angular distances of ca. 90° on the *ac* great circle. This pattern indicates that the lamellae are approximately tautozonally oriented and that they correspond to two sets of the (*h0l*)-planes. The development of the lamellae through the drag fold is homogeneous, unlike the case of this paper. The relative positional relationship between CH and L⊥ in Fig. 12 is regular as a whole, that indicating a homogeneous stress distribution through the fold during the deformation related to the lamellae. According to the rule of the present author, the stress axes, established on the basis of the lamellae fabric diagram in Fig. 12, are drawn uniformly through the fold in such fashion as the axis of maximum compressive stress is parallel to the axial plane and normal to the axis of the fold and the axis of maximum tensile stress is normal to the axial plane, the stress picture being quite different from that for the specimen described in the present paper. Such style of development of the lamellae is similar to that of shear cleavage in homogeneous material. TUTTLE's interpretation about the relation between the lamellae and the drag fold seems not to be probable.

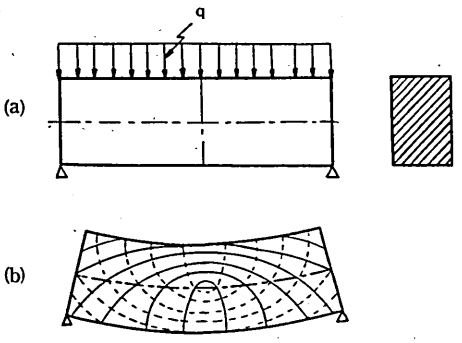

FIG. 13 The lines of principal stress in bending of the simple beam with rectangular cross section under uniform loard (q). (after Kondo, Y., *et al.*, 1959) (b) Solid lines represent the lines of maximum compressive stress and broken lines represent the lines of maximum tensile stress.

Fig. 13 is a stress picture for the maximum compressive and tensile stress in bending of simple beam with rectangular cross section under uniform load (Y. KONDO, *et al.*, 1959). The caluculation is based on the assumptions made in the usual theory of elastic bending. The predicted stress picture is rather similar to the stress picture (drawn with reference to the lamellae) in the knees of the fold I and fold II (Plate 54–4). This fact is surprizing and very interesting. In the knee of the fold I the neutral surface may be drawn along the layer h (mica-rich layer), and in that of the fold II it may be drawn along the layer b

(mica-rich layer). In the fold I and fold II, therefore, the outer knee may be correlated with a tension side of bent beam and the inner knee with a compression side. As mentioned in the preceding page, in Plate 54–4, the stress picture of the left side and that of the right side with reference to the axial plane of the fold are approximately symmetrical. Those evidences seem to indicate that in the deformation related to the lamellae the bending moment rased by a given external force acted as a section force through the fold, and that it acted symmetrically with respect to the axial plane of the fold, unlike the homogeneous two dimensional flattening movement of TUTTLE's case.

As mentioned in the preceding pages, in subarea A the lamellae fabric shows almost perfect orthorhombic symmetry and the two symmetry planes coincide approximately with the fabric planes *ac* and *ab*. The stress system with orthorhombic symmetry responsible for the lamellae fabric has been uniformly established in such fashion as the compression axis is approximately normal to the fabric plane *ab* and the tension axis is approximately parallel to it and normal to the fabric axis *b*. Therefore, the external force acted on the layers of subarea A in the deformation related to the lamellae may be correlated with the uniform load acting normal to the fabric plane *ab*. This should be responsible for the formation of the lamellae in the folded layers of subarea B and C.

Throughout the limbs of the fold the lines of maximum compressive stress are approximately normal to the form surface. Therefore, the neutral surface drawn along the layer h and layer b in the knees of the fold I and fold II respectively can not be traced along those layers towards their limbs. Already at the beginning of the deformation related to the lamellae, the fold in question seems to have almost perfectly attained to its present form.

As described in the preceding page, in some parts of quartz-rich layers develop tiny cracks inclined at high angles to the foliation surface (Plate 54–1). They are of the type of tension crack and are formed subsequently to the formation of the lamellae in quartz grains. Some cracks are filled with micaceous matter injected from the surrounding mica-rich layers (Plate 54–3). The superposition of Plate 54 –1 and 4 indicates that the development of tension cracks through the fold is quite harmonic with the stress system drawn with reference to the lamellae in quartz.

In Plate 54–4 the stress picture for the fold I and that for the fold II are of quite identical fashion. This fact seems to suggest that in the deformation related to the lamellae the quartz-rich layers involved in the fold I reacted independently of those involved in the fold II with respect to a given external force, and that mutual interruption between the former and the latter was lacking. It is obvious that this phenomenon depends upon relative different physical properties of the mica-rich layer d occurring between the fold I and fold II with reference to those of the surrounding quartz-rich layers. At the stage of the deformation related to the lamellae, the mica-rich layer must have been remarkably softer than the quartz-rich layer, and contact strain between the quartz-rich layer (c and e) and

the mica-rich layer (d) was insignificant for unifying the fold I and fold II. The fact that the thicker mica-rich layer d acted as the detachment horizon while that other thinner mica-rich layers did not does not contradict the above statement. In the latter case the intercalated mica-rich layer must have been too thin to vanish the mutual interruption between the separate competent quartz-rich layers.

As described in the preceding pages, the thickness of the mica-rich layers involved in the outer knees of the fold I and fold II is rather constant, while those involved in the inner knees are remarkably thickened in the axial part of knee. The transversal slip cleavages develop in the latter layers, but do not in the former layers. The superposition of Plate 54–1 and 4 indicates that those relationships are quite harmonic with the stress picture for the lamellae in quartz, that is, for the mica-rich layers involved in the "tension side" of the fold knee their thickness is rather constant, and the transversal cleavages do not develop, while those involved in the "compression side" of the fold knee are remarkably thickened in its center and show the transversal cleavages. Dotted lines in the mica-rich layers in Plate 54–4 are approximately normal to the transversal cleavages.

E. Cloos (1947) examined the relation of cleavage and related strain in the study of the recumbent fold of oolitic limestone in South Mountain-fold, Maryland. After him, the transversal cleavages develop in a fan-like arrangement through all the folds, opening towards the anticlinal hinge, and generally parallel to the elongation axes of ooliths. They are well developed in portions distorted more than 20 per cent as measured on the ooliths. The degree of extension of ooliths is commonly less in the upper limb of the recumbent fold than in the lower limb. The relationship between the style of development of the transversal cleavages and the strain ellipsoid (for the deformation related to the formation of the cleavage) drawn with reference to the distortion of ooliths is fairly comparable with that between the transversal cleavages in the mica-rich layers and the stress picture drawn with reference to the lamellae in quartz in the specimen examined in this paper.

IV. Analysis of the Lattice and Dimensional Fabrics of Quartz Grains

The quartz c-axis fabric in the fold in question was examined in 16 sectors shown in Plate 54–5.

Sector 1. The diagram (Fig. 14) is characterized by a sharply defined great circle girdle with two maxima. The great circle girdle coincides with the fabric plane *ac* for the mica fabric and the lamellae fabric in subarea A described in the preceding pages. It shows almost perfect orthorhombic symmetry and the two symmetry planes coincide with the fabric planes *ac* and *ab* for those fabriccs. Thus, the fabric axes (*a*, *b* and *c*) for the mica and the lamellae fabric are available for the quartz c-axis fabric. Angular distance between two maxima is approximately 60° arround the fabric axis *c*. In other words, angular distances between two maxima and the foliation surface together are approximately 60°. As mentioned in the preceding page, in the quartz-rich layers no transversal structural sutface (except tiny tension cracks) has been observed. The two maxima in the diagram do not

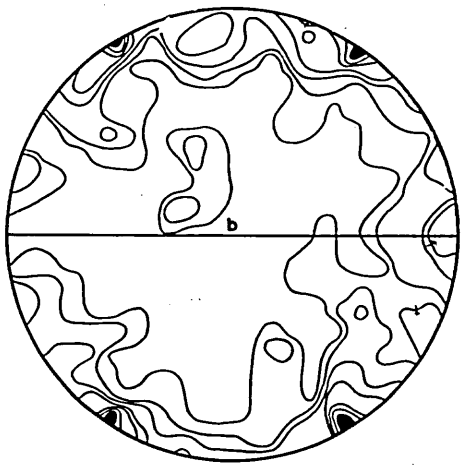

FIG. 14 c-Axes of 200 quartz grains in sector 1 (subarea A). Contours: 7–6–5–4–3–2–1%.

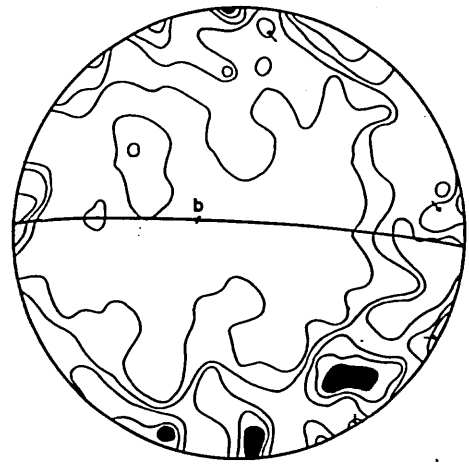

FIG. 15 c-Axes of 100 quartz grains in sector 2. Contours: 5–4–3–2–1%.

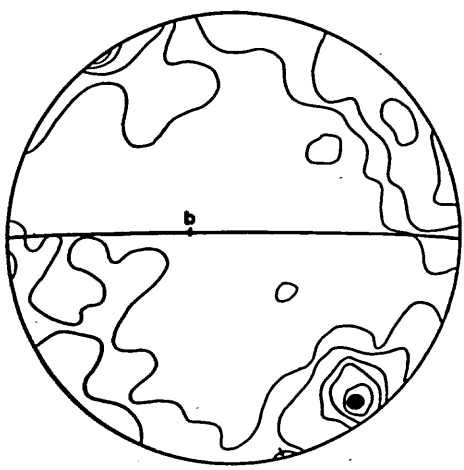

FIG. 16 c-Axes of 100 quartz grains in sector 3. Contours: 11–9–7–5–3–1%.

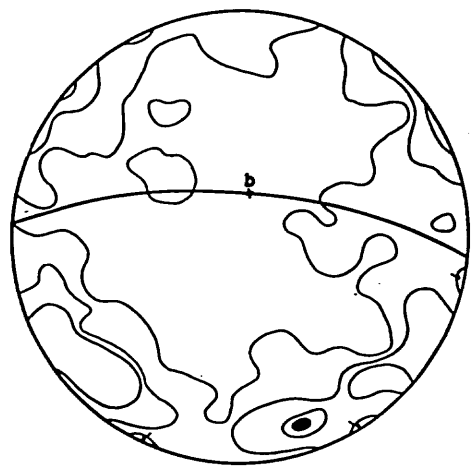

FIG. 17 c-Axes of 80 quartz grains in sector 4. Contours: 7–5–3–1%.

correspond to any position of Maximum I, Maximum II and Maximum V after FAIRBAIRN (1949).

Sector 2. The diagram (Fig. 15) is characterized by a sharply defined great cirdle girdle with three maxima, showing monoclinic symmetry. The great circle girdle coincides with the fabric plane *ac* for the mica fabric and the lamellae fabric in subarea B. The fabric axis *b* for the mica and the lamellae fabric is available for the quartz c-axis fabric. This relationship is equally obvious in all sectors. Maximum angular distance between the maxima is approximately 55°. The center of area containing three maxima on the *ac* great circle is close to the pole of the foliation surface of this sector. They do not correspond to any position of Maximum I, Maximum II and Maximum V after FAIRBAIRN.

Sector 3. The diagram (Fig. 16) is characterized by a sharply defined *ac* great circle girdle with a maximum, showing monoclinic symmetry. Angular distance between the maximum and the foliation surface is approximately 55°.

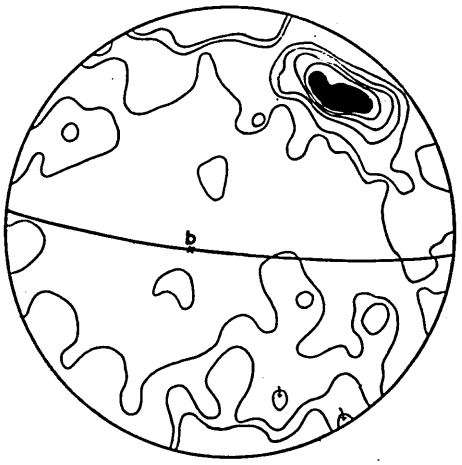

FIG. 18 c-Axes of 100 quartz grains in sector 5. Contours: 6-5-4-3-2-1%.

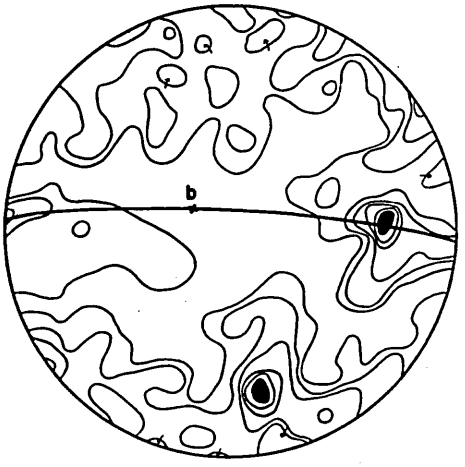

FIG. 19 c-Axes of 100 quartz grains in sector 6. Contours: 6-5-4-3-2-1%.

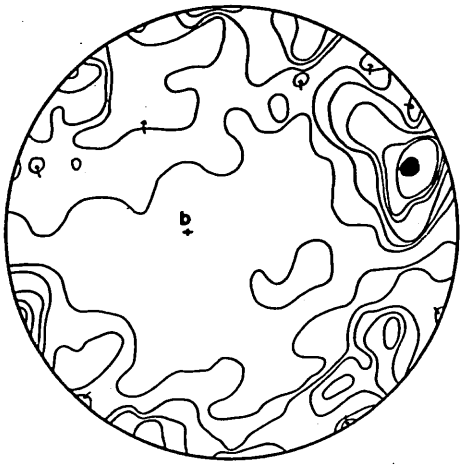

FIG. 20 c-Axes of 100 ouartz grains in sector 7. Contours: 7-6-5-4-3-2-1%.

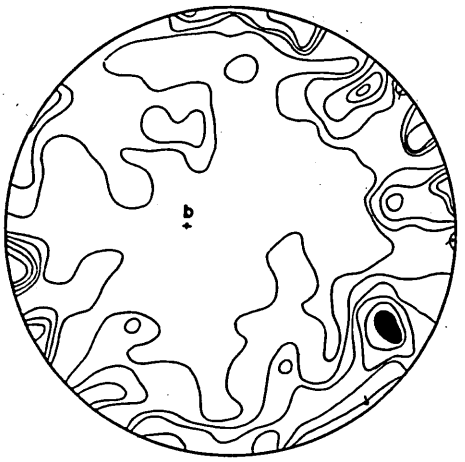

FIG. 21 c-Axes of 100 quartz grains in sector 8. Contours: 6-5-4-3-2-1%.

Sector 4. The diagram (Fig. 17) is characterized by a sharply defined *ac* great circle girdle with a maximum, showing monoclinic symmetry. Angular distance between the maximum and the foliation surface is approximately 70°.

Sector 5. The diagram (Fig. 18) is characterized by a sharply defined *ac* great circle girdle with a maximum, showing monoclinic symmetry. Angular distance between the maximum and the foliation surface is approximately 60°.

Sector 6. The diagram (Fig. 19) is characterized by a sharply defined *ac* great circle girdle with two maxima, showing approximate monclinic symmetry. The one of two maxima shows the position of Maximum I with reference to the foliation surface. Angular distance between the other maximum and the foliation surface is approximately 77°.

Sector 7. The diagram (Fig. 20) is characterized by a sharply defined *ac* great circle girdle with a maximum and a submaximum, showing monoclinic symmetry. Angular distance between the maximum and submaximum is approximately 50°. The middle point between them on the *ac*

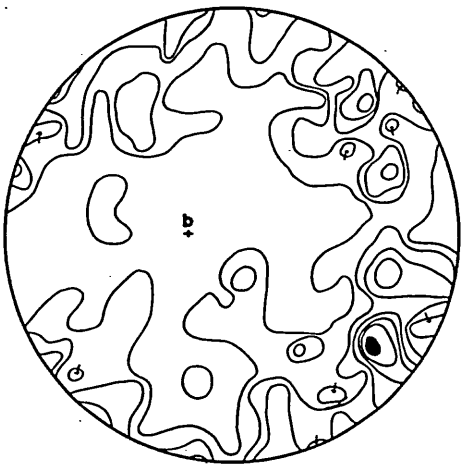

FIG. 22 c-Axes of 100 quartz grains in sector 9. Contours: 6–5–4–3–2–1%.

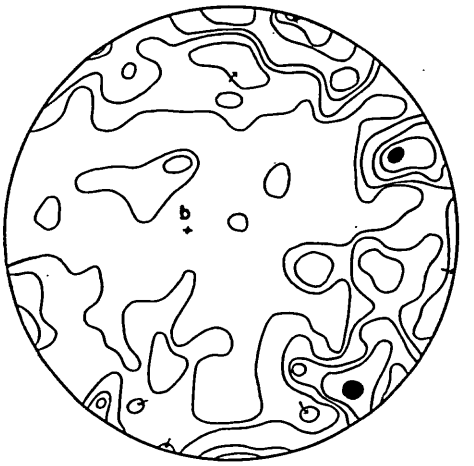

FIG. 23 c-Axes of 100 quartz grains in sector 10. Contours: 5–4–3–2–1%.

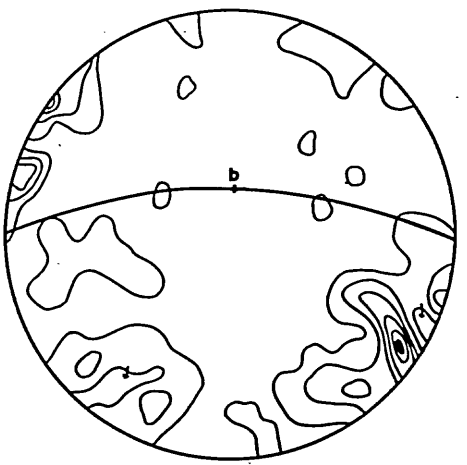

FIG. 24 c-Axes of 60 quartz grains in sector 11. Contours: 10–8–6–5–3–1%.

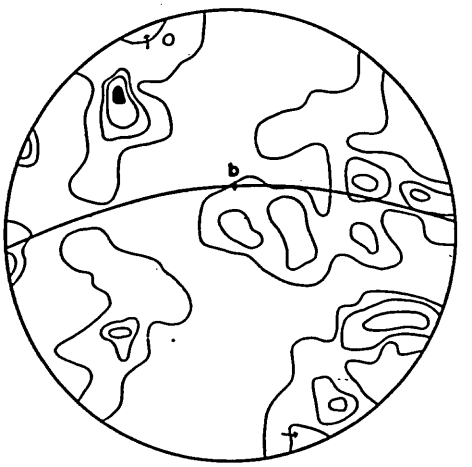

FIG. 25 c-Axes of 60 quartz grains in sector 12. Contours: 7–5–3–1%.

great circle lies approximately on the axial plane of the fold I in this sector.

Sector 8. The diagram (Fig. 21) is characterized by a broad great circle girdle and a maximum and three submaxima. The great circle girdle coincides approximately with the *ac* great circle. The maximum and one submaximum lie on the *ac* great circle, but other two submaxima are present slightly away from it.

Sector 9. The diagram (Fig. 22) is characterized by a sharply defined *ac* great circle girdle with a maximum and three submaxima, showing monoclinic symmetry. The pattern seems to reflect micro-fold of the foliation surface in this sector. The diagram is also characterized by subordinate incomplete girdles containing the maximum and submaxima trending approximately perpendicular to the *ac* great circle.

Sector 10. The diagram (Fig. 23) is characterized by a sharply defined *ac* great circle girdle with two maxima and three submaxima, showing monoclinic symmetry. The pattern seems to reflect micro-fold of the foliation surface in this sector. The maximum areas and submaximum areas in the

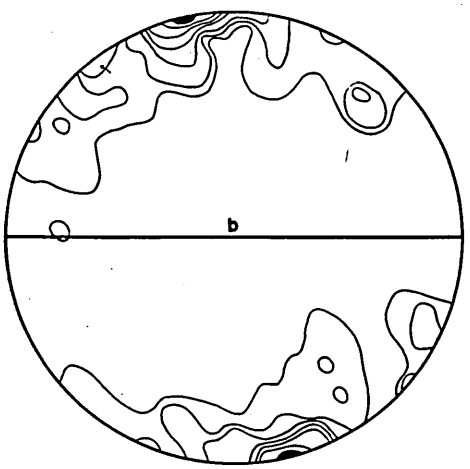

FIG. 26 c-Axes of 80 quartz grains in sector 13. Contours: 9–7–6–5–4–3–1%.

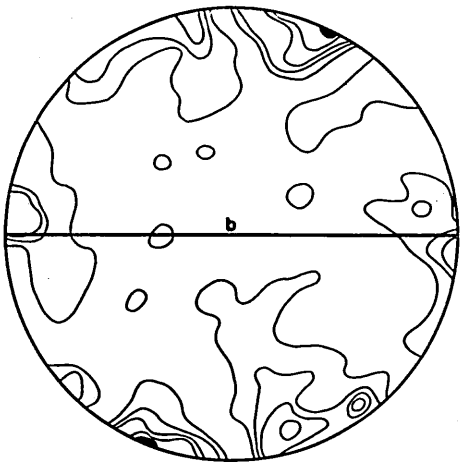

FIG. 27 c-Axes of 70 quartz grains in sector 14. Contours: 7–6–4–3–1%.

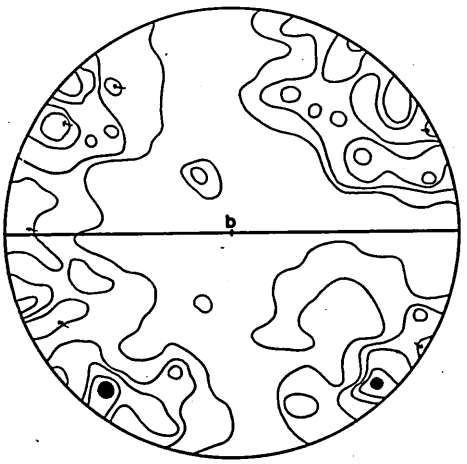

FIG. 28 c-Axes of 70 quartz grains in sector 15. Contours: 7–6–4–3–1%.

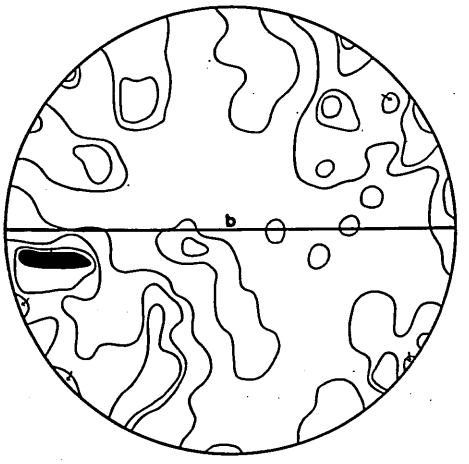

FIG. 29 c-Axes of 100 quartz grains in sector 16. Contours: 4–3–2–1%.

diagram are markedly elongated approximately perpendicular to the *ac* great circle.

Sector 11. The diagram (Fig. 24) is charcterized by an incomplete *ac* great circle girdle with a maximum, showing monoclinic symmetry. Angular distance between the maximum and the foliation surface is approximately 30°. The maximum area in the diagram is markedly elongated approximately perpendicular to the *ac* great circle.

Sector 12. The fabric pattern is triclinic (Fig. 25). Many of c-axes of quartz in the diagram tend to concentrate about a small circle with an angular radius of ca. 60°. A maximum and two submaxima lie on the small circle, the center of which coincides approximately with the fabric axis *b* for the mica fabric and the lamellae fabric in subarea B. Another two submaxima lie on the *ac* great circle. The diagram is also characterized by subordinate incomplete girdles containing the maximum and submaxima trending approximately perpendicular to the *ac* great circle.

Sector 13. The diagram (Fig. 26) is characterized by an incomplete great circle girdle wih a strong maximum, showing monoclinic symmetry. The great circle girdle coincides with the fabric plane

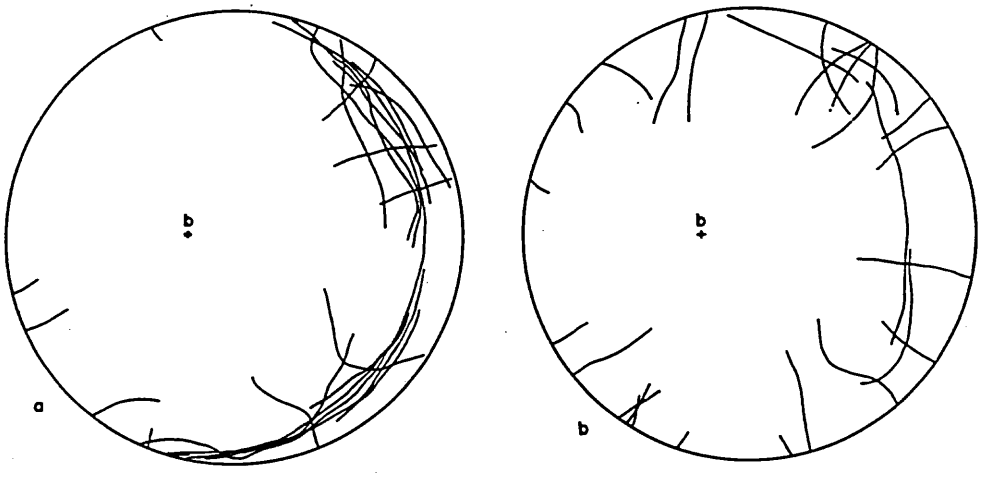

FIG. 30 Diagrams showing the trends of the girdles containing the maxima and submaxima
a) data for the limbs and outer knee of the fold I (sectors 2, 3, 4, 5, 6, 7 and 8)
b) data for the inner knee of the fold I (sectors 9, 10, 11, and 12)

ac for the mica fabric and the lamellae fabric in subarea C. Angular distance between the maximum and the foliation surface is approximately 75°.

Sector 14. The diagram (Fig. 27) is characterized by an incomplete *ac* great circle girdle with a maximum and two submaxima. The two submaxima seem to have no separate significance and may be grouped together as one submaximum group. Angular distance between the maximum and submaximum group is approximately 50°. The middle point between them on the *ac* great circle is approximately perpendicular to the foliation surface in this sector.

Sector 15. The fabric pattern is triclinic (Fig. 28). Many of c-axes of quartz in the diagram tend to be rather present slightly away from the *ac* great circle, that showing an incomplete broad girdle, center of which coincides with the fabric axis *b* for the mica fabric and the lamellae fabric in subarea C.

Sector 16. The fabric pattern is triclinic (Fig. 29). Many of c-axes of quartz tend to concentrate in an incomplete small circle girdle with a maximum and a submaximum with an angular radius of ca. 60°, center of which coincides with the fabric axis *b* for the mica fabric and the lamellae fabric in subarea C. Angular distance between the maximum and submaximum is approximately 50°. The maximum area and submaximum area in the diagram are markedly elongated approximately perpendicular to the *ac* great circle. The maximum is close to the position of Maximum I with reference to the foliation surface.

On the basis of symmetrological analysis of the c-axis fabrics in the preceding pages, it can be safely pointed out that in each subarea the fabric axis *b* for the mica fabric and the lamellae fabric coincides practically with that for the c-axis fabric, therefore that in the deformation related to the formation of the c-axis fabric the layers involved in the fold moved independently of the surrounding non-folded layers, and further that the layers involved in the fold I moved independently of those involved in the fold II, as in the deformations related to the mica fabric and the lamellae fabric. In subarea A the c-axis fabric shows almost perfect orthohombic symmetry as well as the lamellae fabric, while in subareas B and C it shows monoclinic or triclinic symmetry, that indicating distinct discrep-

ancy between subarea A and subareas B and C with respect to the stress and movement picture in the deformation related to the c-axis fabric.

The c-axis fabric through the fold is not homogeneous, and also each diagram does not always show similar pattern. However, the fabric diagrams from the outer knees and limbs of the fold I and fold II are correlated with each other in essential nature of fabric pattern, and also those from the inner knees of both folds show similar pattern in essential points. While, between the former and the latter is detected distinct difference. The c-axis fabrics from the outer knees and limbs are commonly characterized by a sharply defined *ac* great circle girdle with maximum and submaximum, showing monoclinic symmetry, while in those from the inner knees the number of c-axis of quartz on the *ac* great circle girdle decrease and many of them tend to concentrate rather on an *ac* small circle girdle slightly (30°-) away from the *ac* great circle. The triclinic symmetry of fabric pattern is recognized in some diagrams from the inner knees. Fig. 30-a and b are diagrams for the trends of the girdles containing the maxima and submaxima in the c-axis diagrams from the outer knee and limbs and from the inner knee of the fold I respectively. When Fig. 30-a and b are compared, the discrepancy between the c-axis fabrics from the former and those from the latter is distinct. Fig. 30-b indicates that in the c-axis diagrams from the inner knee incomplete girdles trending approximately perpendicular to the *ac* great circle are of characteristic feature. Those evidences suggest that in the deformation related to the c-axis fabrics the stress and movement picture in the outer knees and limbs were quite different from those in the inner knees.

Angular distances between the observed structural surface (single set of foliation surface as the form surface of the fold) and maxima and submaxima in each diagram examined in the preceding pages can not be illustrated in terms of preferred orientation of common crystallographic planes of quartz on the foliation surface (SANDER, 1930, 1950; FAIRBAIRN, 1949; KOJIMA and HIDE, 1958). The author (1961a) pointed out that the c-axis of quartz may stably be oriented at an angle of ca. 30° to the greatest contraction axis in the system concerned or of ca. 60° to the greatest extension axis. On the basis of this hypothesis, the pattern of small circle girdle with an angular radius of ca. 60°, which is most commonly seen in the literature reported so far, was correlated with the extension parallel to the axis perpendicular to the girdle, accompanied with equal amount of contraction in all the directions within the plane perpendicular to the extension axis (HARA, 1962). This type of c-axis fabric is commonly associated with subordinate incomplete girdles containing the maxima and submaxima trending approximately perpendicular to the small circle. They were interpreted as to reflect the reorientation of initial fabrics under newly induced stress condition.

The author's hypothesis described above may be applicable to the c-axis fabrics in question. According to the hypothesis, the c-axis fabric showing orthorhombic symmetry in subarea A seems to be correlated with a strain picture having ortho-

rhombic symmetry such as the axis of maximum contraction is approximately normal to the fabic plane *ab* and the axis of maximum extension is parallel to the fabric axis *a*. The strain picture is quite harmonic with that for the lamellae in quartz above described. Of course, the lamellae in quartz are a structure of later stage unrelated to the deformation which induced the lattice and dimensional fabrics to the quartz grains.

Plate 54–6 indicates superposition of the compression axis for the lamellae and the c-axis fabrics through the fold. In sectors 2, 3, 4, 5, 7, 8, 9, 10, 11, 13, and 14, the strain picture for the c-axis fabric can be established in harmonic fashion with that for the lamellae. Broadly speaking, in the outer knees and limbs the strain picture in the deformation related to the c-axis fabrics can be established in such fashion as the axis of maximum contraction is approximately normal to the form surface of the fold and the axis of maximum extension is approximately parallel to it and normal to the fabric axis *b*. In the c-axis diagram of sector 6 angular distance between two maxima is approximately 80°. The two maxima may respectively be correlated with separate deformation. The one is Maximum I with reference to the foliation surface, and the other is close to the average direction of the compression axis for the lamellae in this sector (Plate 54–6). In the c-axis diagrams of sectors 12, 15 and 16, especially of sectors 12 and 16, the fabric pattern is commonly characterized by a broad *ac* small circle girdle and subordinate girdles trending subnormal to it, that suggesting the secondary axial extension parallel to the fabric axis *b*. The strain picture is different from that for the lamellae in these sectors and that for the c-axis fabrics in other sectors examined just above. Also in the c-axis diagrams from the outer part of the inner knees (sectors 9 and 10) larger amount of c-axes of quartz distributes in an *ac* small circle girdle slightly away from the *ac* great circle, when compared with those from the outer knees and limbs. Passing from the outer knee to the innermost knee, amount of c-axes of quartz in the *ac* small circle girdle progressively increases, that probably representing gradual change of the stress picture. In the knees of the fold I and fold II the neutral surface may be drawn along the layer h and layer b respectively. The strain picture for the c-axis fabrics through the fold I and fold II examined above seems to be well correlated with that in the experimental bending of prisms. Already at the stage of printing of the c-axis fabrics observed now, the fold in question seems to have almost perfectly attained to its present form. The maximum in the diagram of sector 6 (Fig. 19), which is Maximum I with reference to the foliation surface, may be a relict of the maximum induced at the earlier stage of the folding.

The strain picture for the c-axis fabrics in the fold I and that in the fold II are of quite identical fashion. This relationship suggests that in the deformation related to the c-axis fabric the quartz-rich layers involved in the fold I reacted independently of those involved in the fold II with respect to a given external force, and the mutual interruption between the former and the latter was effectively

lacking, as in the deformation related to the lamellae in quartz. Also at the stage of the deformation related to the c-axis fabrics, the mica-rich layer must have been remarkably softer than the quartz-rich layer, and contact strain between the quartz-rich layer (c and e) and mica-rich layer (d) was insignificant.

Fold of the quart-rich layer i containing sectors 3, 4, 5, 7 and 8, which corresponds to the middle to outer horizon of the fold I, appears to be clearly illustrated also with reference to the petrofabric technique of fold analysis after LADURNER (1954a). The c-axis diagrams of sectors 3, 4 and 5, that correspond to the limb, show a single marked maximum, as shown in Figs. 16, 17 and 18. Angular distance between the maximum and the foliation surface is not constant, between 55° and 70°. The q-Richtung after LADURNER can be established with certainty in each diagram. The q-Richtungen are approximately fan-shaped in distribution through the fold (of layer i), as read in Plate 54–6. When the fold (of layer i) is partially unfolded until the correlated q-Richtungen are aligned parallel to one another, a shallow troughed fold form is obtained, as is obvious when Figs. 16, 17 and 18 are compared. Thus, if it is probable that the pattern of the c-axis diagrams of sectors 7 and 8 reflects the influence of micro-fold of foliation surface in the axial part of the fold knee, the fold of the layer i in question may be illustrated in terms of K. A. JONES (1959), "The symmetrical arrangement of the q-Richtungen, that is the symmetrical orientation of quartz maxima to the fold knee in both flanks, indicates that these q-directions were already in existence before the bending to form a heterogenous fabric. The fold thus attained its present form through a period of shearing, giving rise to the form as reconstructed in the partially unfolded state, followed by flexure folding with retention of the old fabric axis and the "*ac*" symmetry". However, this illustration is not applicable to the c-axis fabrics throughout whole examined area (the fold I, fold II and unfolded zone). Therefore, LADURNER's technique of fold analysis seems not always to be applicable in synthesizing mechanics of folding even when a single marked maximum occurs in the c-axis diagram.

The dimensional fabric of quartz grains in the quartz-rich layers was examined on the thin section normal to the axis of the fold II. In Fig. 31 is shown the diagram for the variation in the angle between the elongation axis of quartz grain and the foliation surface and for the relationship between the angular deviation of the elongation axis from the foliation surface and the degree of elongation for 50 grains in sectors 3, 7, 11, 12, 14 and 15. In sectors 3, 7 and 14, many of quartz grains are preferably oriented with their longest dimension parallel to the foliation surface, and show markedly tabular habit. Analogous relation of the dimensional fabric is equally obvious for quartz grains in the quartz-rich layers of subarea A, for those in the layers c, i, k, m, o and q, and for those in parts (corresponding to the fold limbs) of layers e and g. The dimensional fabrics of quartz grains in sectors 11 and 12 is illustrated in Fig. 31-(11, 12). In the innermost knee of the fold I, the longest axes of quartz grains have random orientation, and their shapes

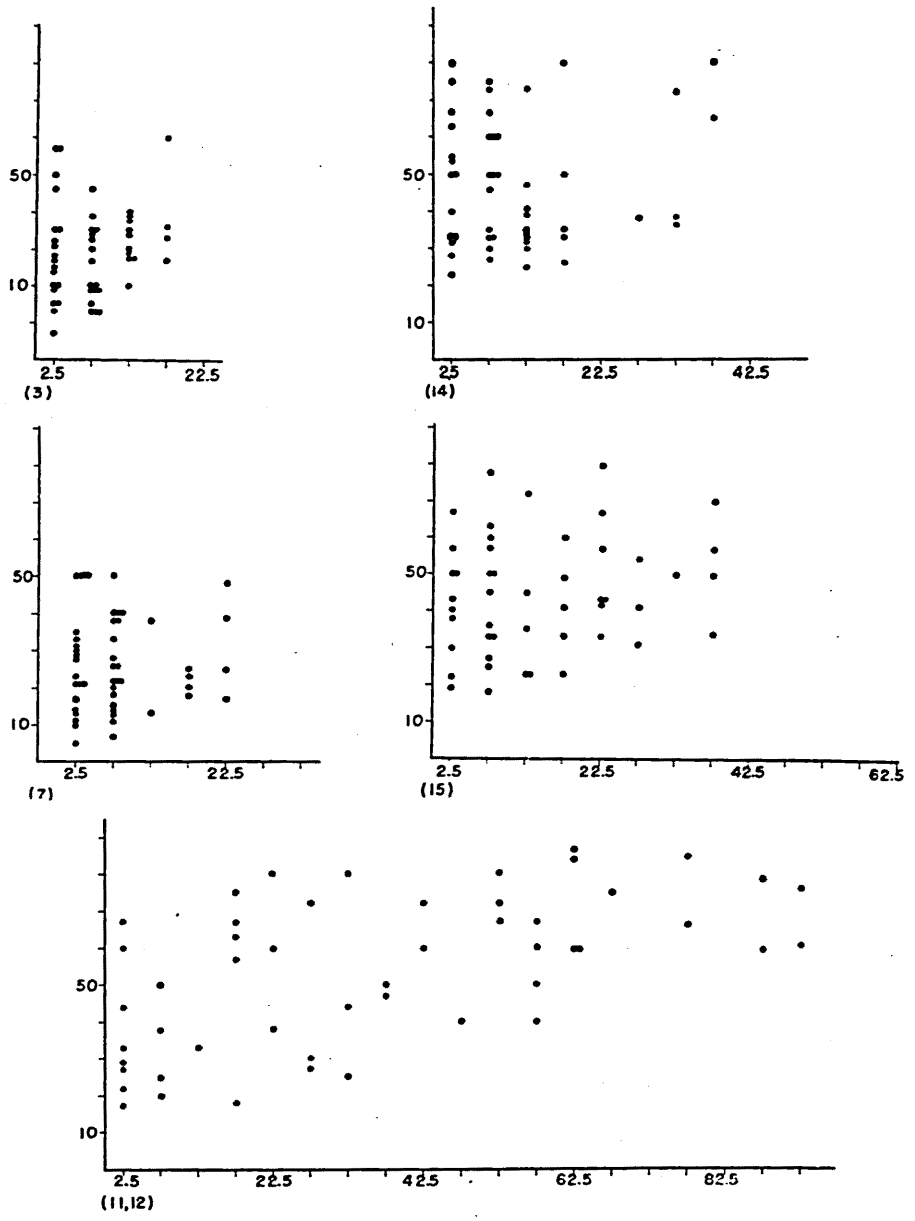

FIG. 31 Diagram for the variation in the angle between the elongation axis of quartz grain and the foliation surface and for the relation between the angular deviation of the elongation axis from the foliation surface and degree of elongation for the quartz grains in sectors 3, 7, 11, 12, 14 and 15.

the ordinates : $\underset{(X)}{\frac{100}{X}} = \frac{\text{the longest dimension}}{\text{dimension normal to the longest dimension}}$

the abscissas : the angle between the elongation axis of grain and foliation surface

are commonly less tabular. Fig. 31-(15) is the data for sector 15. The preferred orientation of elongated quartz grains along the foliation surface is not so remarkable, when compared with that in sectors 3, 7 and 14 described above. The dimensional fabric in sectors 8, 9 and 10 is similar to that in sector 15, though data for these sectors were not described in this paper. Broadly speaking, between the dimensional fabric of quartz grains in the limbs and outer knees of the fold I and fold II and that in their inner knees is detected distinct difference. In the former parts, many of quartz grains are preferably oriented with their longest dimension parallel to the foliation surface, and show markedly tabular habit. While, in the latter parts, the longest axes of quartz grains have less regular orientation, and their shapes are less tabular. Above described features of the dimensional fabric of quartz grains must be correlated with a certain stress system acted through the fold. FAIRBAIRN (1950) observed the elongation of quartz grains normal to the compression axis in the experimental deformation of quartz sand. The strain picture drawn with reference to the dimensional fabrics of quartz grains through the outer knees and limbs of the fold I and fold II, according to the experimental result after FAIRBAIRN, is comparable with that for the lamellae fabric and the c-axis fabric discussed in the preceding pages. While, the fabric pattern in the inner knees of the fold I and fold II can not well be correlated with a certain appropriate strain picture. This fact may indicate that the dimensional fabric of quartz grains was not well reconstructed at the stage of the deformation which produced the c-axis fabric observed now.

REFERENCES

BAILEY, S. W., BELL, R. A. and PENG, C. J. (1958) : Plastic deformation of quartz in nature. *Geol. Soc. America Bull.*, **69**, 1443–1460.

BALL, T. K. (1960) : A petrofabric analysis of a fold. *Am. Jour. Sci.*, **258**, 274–281.

CHRISTIE, J. M. and RALEIGH, C. B. (1959) : The origin of deformation lamellae in quartz. *Am. Jour. Sci.*, **257**, 358–407.

CLOOS, E. (1947) : Oolite deformation in the South Mountain-fold, Maryland. *Geol. Soc. America Bull.*, **58**, 843–918.

DORN, J. E. (editor) (1961) : *Mechanical behaviour of materials at elevated temperature.* New York.

FAIRBAIRN, H. W. (1939) : Correlation of quartz deformation with its crystal structure. *Am. Mineralogist*, **24**, 351–368.

——— (1941) : Deformation lamellae in quartz from the Ajibik formation, Michigan. *Geol. Soc. Ameraca Bull.*, **52**, 1265–1277.

——— (1949) : *Structural petrology of deformed rocks.* Cambridge, Mass., Addison and Wesley Publishing Co.

——— (1950) : Synthetic quartzite. *Am. Mineralogist*, **35**, 735–748.

FISHER, G. (1925) : Mechanisch bedingte Streifungen an Quarz. *Zentralblatt Min. Geol. Pal.*, Abt. A. (7), 210–213.

GRIGGS, D. T. and BELL, J. F. (1938) : Experiments bearing on the orientation of quartz in deformed rocks. *Geol. Soc. America Bull.*, **49**, 1723–1746.

HARA, I. (1961a) : Dynamic interpretation of the simple type of calcite and quartz fabrics in the naturally deformed calcite-quartz vein. *Jour. Sci. Hiroshima Univ. Series* C. **4**, 35–54.

——— (1961b) : Petrofabric study of the lamellar structures in quartz. *Jour. Sci. Hiroshima Univ., Series* C. **4**, 55–70.

——— (1962) : Studies on the structure of the Ryôke metamorphic rocks of the Kasagi district, Southwest Japan. *Jour. Sci. Hiroshima Univ., Series* C. **4**,

HIETANEN, ANNA (1938) : On the petrology of the Finnish quarzites. *Comm. Geol. de Finlande Bull.* (122), 118.

INGERSON, E. (1940) : Fabric cirteria for distinguishing pseudo-ripple marks from ripple marks. *Geol. Soc. America Bull.*, **51**, 557–570.

INGERSON, E. and TUTTLE, O. F. (1945) : Relations of lamellae and crystallography of quartz and fabric directions in some deformed rocks. *Am. Geophrs. Union Trans.*, **26**, 95–105.

JONES, K. A. (1959) : A petrofabric method of fold analysis. *Am. Jour. Sci.*, **257**, 138–143.

KOJIMA, G. and HIDE, K. (1958) : Kinematic interpretation of the quartz fabric of triclinic tectonites from Besshi, Shikoku, Japan. *Jour. Sci. Hiroshima Univ., Series* C, **2**, 195–226.

KONDO, Y. and KODAMA, T. (1959): *Mechanics of Materials* (in Japanese). Kokuminkagakusha Tokyo.

LADURNER, J. (1954a) : Beitrage zur Typisierung von Quarzfalten. *Tschermaks Mineralog. Petrog. Mitt.*, F. 3, Bd. **2**, 47–66.

——— (1954b) : Beiträge zur Typisierung von Falten. II. Calcitfalten. *Tschermaks Mineralog. Petrog. Mitt.*, Bd. **IV**/1–4, 34–43.

MÜGGE, O. (1896) : Der Quarzporphyr der Bruchhauser-Steine in Westfalen. *Neues Jahrb. Mineralogie*, 757–787.

PRESTON, J. (1958) : Quartz lamellae in some Finnish quartzites. *Comm. Geol. de Finlande Bull.*, (180), 65–78.

SANDER, B. (1930) : *Gefügekunde der Gesteine.* Vienna, Springer Verlg.

——— (1950) : *Einführung in die Gefügekude der geologischen Körper*, IIer Teil, Die Korngefüge. Wien und Innsbruck.

SCHMIDT, W. (1927) : Untersuchung über die Regelung des Quarzgefüges kristalliner Schiefer. *Fortschr. der Mineraloge.* Bd. **11**, 27–29.

SITTER, L. U. De (1956) : *Structural geology.* New York.

TURNER, F. J. and CH' IH, C. S. (1951) : Deformation of Yule marble : part III-Observed fabric changes due to deformation at 10,000 atmospheres confining pressure, room temperature, dry. *Geol. Soc. America Bull.*, **62**, 887–905.

TURNER, F. J. (1953) : Nature and dynamic interpretation of deformation lamellae in calcite of three marbles. *Am. Jour. Sci.*, **251**, 276–298.

TUTTLE, O. F. (1949) : Structural petrology of planes of liquid inclusions. *Jour. Geology*, **57**, 331–356.

WEISS' L. E. (1954) : A study of tectonic style : Structural investigation of a marble-quartzite complex in southern California. *Univ. California, Publication in Geological Science*, **30**, 1–102.

ZOZMANN, I. S. (1955) : Gefügeanalysen an Quarzfalten. *Neues Jahrb. Mineralogie.* **87**, 321–350.

INSTITUTE OF GEOLOGY AND MINERALOGY,
FACULTY OF SCIENCE, HIROSHIMA UNIVERSITY

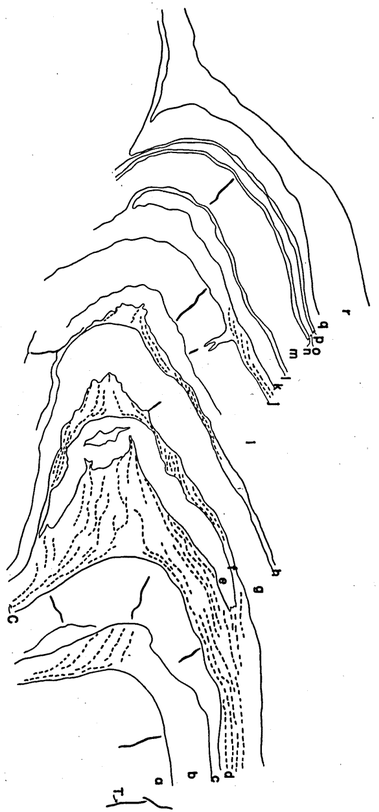

FIG. 1. Skecth of the fold (investigated area). a, b, c, ··· r: name of layer. C: transversal slip cleavage. T: tension crack.

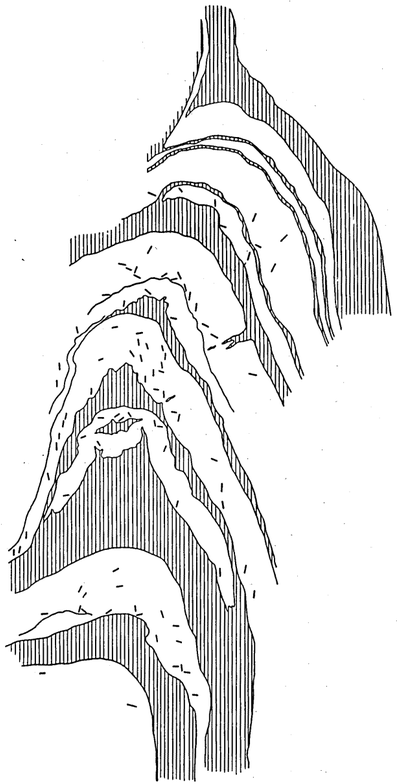

FIG. 2. The distribution of grains containing the lamellae through the fold and the trend of the lamellae in each grain.

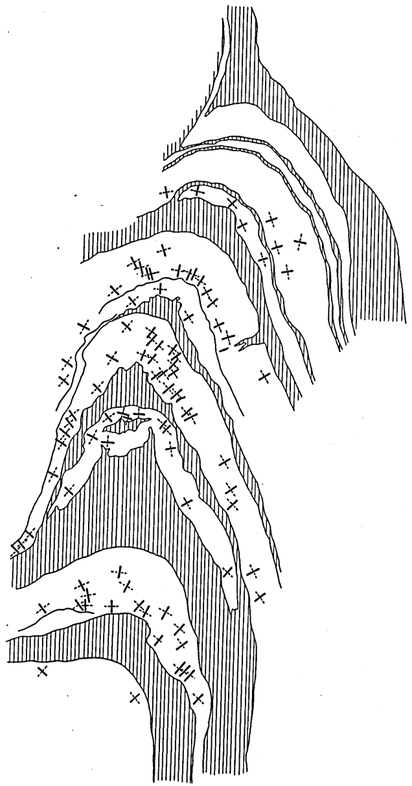

FIG. 3. The compression (—) and tension axis (---) for the lamellae in individual grains in Fig. 2.

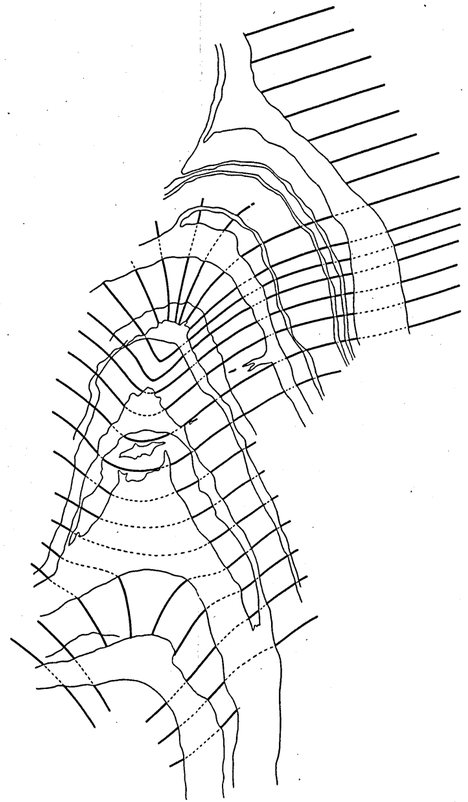

FIG. 4. The lines of maximum compressive stress through the quartz-rich layers in the fold drawn with reference to Fig. 3.

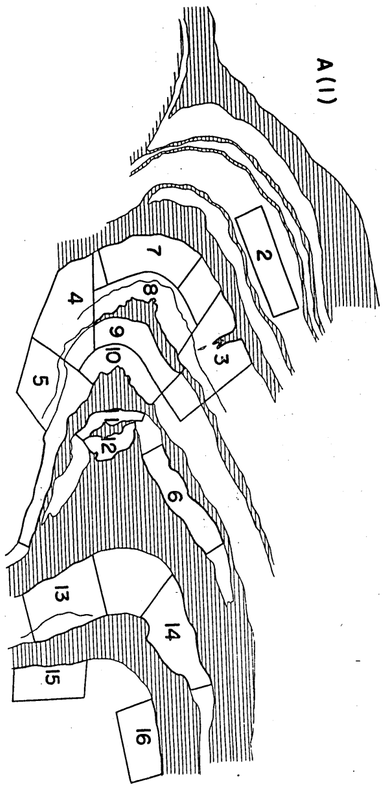

FIG. 5. Diagram of fold showing position of 15 sectors.

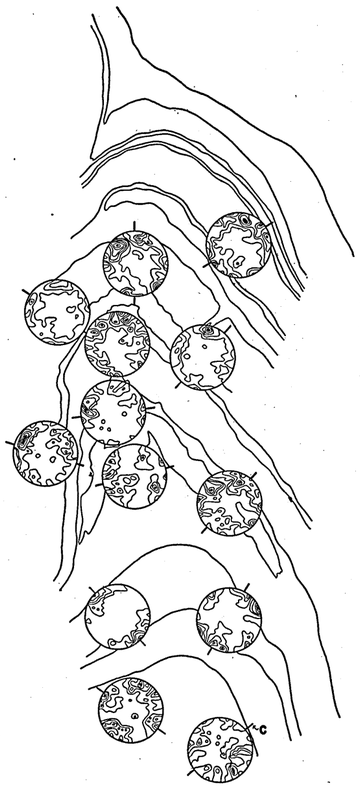

FIG. 6. Superposition of the c-axes fabrics and the lines of maximum compressive stress for the lamellae through the fold. C: the average direction of the lines of maximum compressive stress in each sector.

Explanation of Plate LV

Fig. 1. Profile of the fold (in part). Crossed nicols.
Fig. 2. Profile of the fold (in part). Lower nicol only.
Fig. 3. Tension crack filled with micaceous matter which intruded from the adjacent mica-rich layer. Lower nicol only.
Fig. 4. The lamellae of Type L1. Crossed nicols.
Fig. 5. The lamellae of Type L3. Crossed nicols.

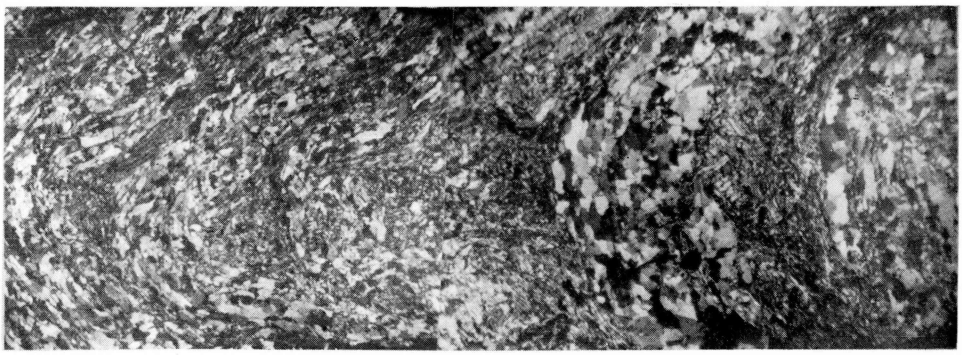

FIG. 1

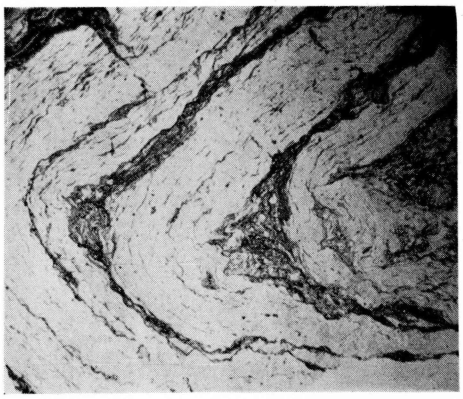

FIG. 2

FIG. 3

FIG. 4

FIG. 5